JPn Neuroscience

The Journal of Physiology

J Physiol 594.19 (2016) pp 5685–5694

Time course of EPSCs in ON-type starburst amacrine cells is independent of dendritic location

Todd Stincic[1], Robert G. Smith[2] and W. Rowland Taylor[1]

[1] *Department of Ophthalmology, Casey Eye Institute, Oregon Health & Science University, Portland, OR 97239, USA*
[2] *Department of Neuroscience, University of Pennsylvania, Philadelphia, PA 19104, USA*

Key points

- Direction selectivity has been widely studied as an example of a complex neural computation.
- Directional GABA release from starburst amacrine cells (SBACs) is critical for generating directional signals in direction-selective ganglion cells. The mechanisms producing the directional release remain unclear.
- For SBACs, ordered distribution of sustained and transient bipolar cell inputs along the dendrites is proposed to generate directional GABA release. This study tests whether this hypothesis applies to ON-type SBACs.
- EPSCs activated at proximal and distal dendritic locations have the same time course. Therefore, the ordered arrangement of inputs from bipolar cells with different kinetic properties cannot be responsible for generating directional GABA release from ON-type SBACs.

Abstract Direction selectivity in the retina relies critically on directionally asymmetric GABA release from the dendritic tips of starburst amacrine cells (SBACs). GABA release from each radially directed dendrite is larger for motion outward from the soma toward the dendritic tips than for motion inwards toward the soma. The biophysical mechanisms generating these directional signals remain controversial. A model based on electron-microscopic reconstructions of the mouse retina proposed that an ordered arrangement of kinetically distinct bipolar cell inputs to ON- and OFF-type SBACs could produce directional GABA release. We tested this prediction by measuring the time course of EPSCs in ON-type SBACs in the mouse retina, activated by proximal and distal light stimulation. Contrary to the prediction, the kinetics of the excitatory inputs were independent of dendritic location. Computer simulations based on 3D reconstructions of SBAC dendrites demonstrated that the response kinetics of distal inputs were not significantly altered by dendritic filtering. These direct physiological measurements, do not support the hypothesis that directional signals in SBACs arise from the ordered arrangement of kinetically distinct bipolar cell inputs.

(Received 3 March 2016; accepted after revision 19 May 2016; first published online 24 May 2016)
Corresponding author W.R. Taylor: Casey Eye Institute, Oregon Health and Science University, 3375 SW Terwilliger Blvd, Portland, OR 97239, USA. Email: taylorw@ohsu.edu

Abbreviations BC, bipolar cell; DSGC, direction selective ganglion cell; EM, electron micrograph; SBAC, starburst amacrine cell.

Introduction

Direction-selective ganglion cells have been widely studied in the mammalian retina as an example of neural computation in the early visual system (Barlow & Hill, 1963; Barlow *et al.* 1964). Initial investigations demonstrated that directional signalling in these ganglion cells required GABAergic inhibition (Wyatt & Daw, 1976;

DOI: 10.1113/JP272384

Caldwell *et al.* 1978; Kittila & Massey, 1997). Subsequent analysis showed that the critical inhibition arises from starburst amacrine cells (SBACs) (Yoshida *et al.* 2001), and that these cells make selective contacts with direction selective ganglion cells (DSGCs), such that the directional release of GABA is selectively targeted to the null side of a DSGC dendritic arbour (Fried *et al.* 2002; Lee *et al.* 2010; Briggman *et al.* 2011). Thus directional spike generation is dependent on directional inhibition impinging on the DSGCs. Ca^{2+} imaging studies have shown that each radially directed SBAC dendrite displays larger GABA release for motion directed outward from the soma (Euler *et al.* 2002; Lee & Zhou, 2006). While several mechanisms have been proposed to underlie this directional GABA release, none have proved definitive (Ozaita *et al.* 2004; Tukker *et al.* 2004; Lee & Zhou, 2006; Hausselt *et al.* 2007; Enciso *et al.* 2010).

Recent studies have proposed a novel mechanism based on anatomical data from scanning block-face electron microscopic reconstruction of the mouse retina, which showed that there is an ordered arrangement of excitatory bipolar cell inputs to SBACs that could generate directionally asymmetric GABA release (Kim *et al.* 2014; Greene *et al.* 2016). For OFF-type SBACs the data showed that much of the excitatory input derived from only two types of bipolar cell and that the inputs from these cells were not randomly distributed along the dendritic branches; Type-2 bipolar cells make input selectively to the proximal dendrites of SBACs, while Type-3a cells make inputs more distally (Kim *et al.* 2014). For ON-type SBACs an analogous arrangement was observed with Type-7 and Type-5 bipolar cells fulfilling the roles of sustained and transient inputs, respectively (Greene *et al.* 2016). These bipolar cells had previously been identified in imaging studies as having sustained and transient response properties, respectively (Baden *et al.* 2012; Borghuis *et al.* 2013). Combining these anatomical and physiological data, it was proposed that directional output from the SBACs arose from asymmetric superposition of excitation in the distal dendrites of the SBACs where GABA release occurs; as an edge moves outward, the sustained signal from Type-2/7 cells (BC2/7) at the base, would sum synergistically with subsequent activation of the transient inputs from Type-3a/5 cells (BC3a/5) in the outer dendrites (Fig. 1). For motion in the opposite direction, towards the soma, the transient inputs would decay before recruitment of the sustained input, and the depolarization at the dendritic tips, and hence GABA release, would be weaker. We will refer to this arrangement as the 'ordered-input' model. This paper tests this hypothesis by making voltage-clamp recordings of light-evoked excitatory postsynaptic currents (EPSCs) from ON-type SBACs in the mouse retina.

Methods

All procedures involving animals complied with the National Institutes of Health guidelines for animal use and a protocol approved by the Institutional Animal Care and Use Committee at Oregon Health & Science University. Fifteen mice were used (C57BL/6J, strain 000664), ranging from 4 weeks to 4 months of age; three males and two females for the modelling experiments, and 10 males for the physiology experiments. Mice were from onsite colonies established with founders from The Jackson Laboratory (Bar Harbor, ME, USA). Animals had *ad libitum* access to food and water and were kept on a 12/12 light/dark cycle. Experiments were performed during the circadian day. Mice were dark-adapted for at least 1 h prior to isolating the retinas. The animals were deeply anaesthetized by intraperitoneal injection of sodium pentobarbital (0.25 ml, 50 mg ml^{-1}) and killed by cervical dislocation immediately following enucleation. Retinas were isolated and maintained under dim red or infra-red illumination for all subsequent procedures.

Electrophysiology

Starburst amacrine cells were voltage-clamped through an electrode applied to the soma. Patch electrodes were pulled from borosilicate glass to a final resistance of 4–8 MΩ and were filled with an intracellular solution containing (in mM): 128 methane sulfonate, 6 CsCl, 10 Na-Hepes, 1 EGTA, 2 Mg-ATP, 1 Na-GTP, 5 phosphocreatine, 3 QX-314, and 0.1 spermine. The pH was adjusted to 7.4 with CsOH. Reagents were obtained from Sigma-Aldrich (St Louis, MO, USA) unless otherwise indicated. To improve voltage-clamp at positive potentials, potassium was replaced by caesium in order to block voltage-gated

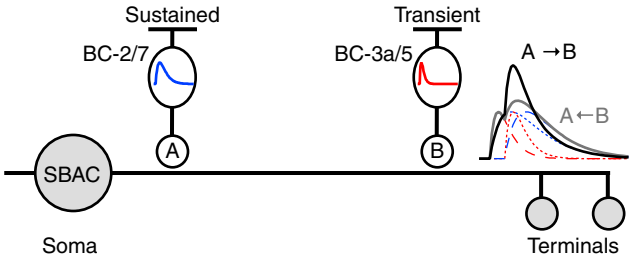

Figure 1. Schematic diagram of the ordered-input model
Sustained bipolar cells BC-2 (OFF) and BC-7 (ON) selectively contact the proximal dendrites. Transient bipolar cells BC-3a (OFF) and BC-5 (ON) selectively contact the distal dendrites. The hypothetical kinetics is shown, sustained in blue and transient in red. For outward motion (A→B, black trace) the delayed transient input sums with the sustained response activated earlier. For inward motion (B→A, grey trace) the sustained input is activated after the transient one has largely decayed.

potassium currents. Voltages were adjusted by –10 mV to correct for the liquid junction potential.

Radial cuts were made on retina halves to facilitate flat mounting on Whatman Anodiscs, which were then placed in a recording chamber and held in place with a harp. The preparation was constantly perfused with Ames medium (United States Biological, Salem, MA, USA) at a flow rate of 3–4 ml min^{-1} maintained at 32–34°C.

Light stimulation and recording

Stimuli generated on CRT computer monitors at refresh rates of 60 or 85 Hz were projected through the ×20 water-immersion microscope objective (NA = 0.95) onto the photoreceptor outer segments. Percentage contrast was defined as $C = 100(L_{max} - L_{min})/(L_{max} + L_{min})$, where L_{max} and L_{min} are the maximum and minimum intensities of the stimulus, respectively. The retina was adapted to photopic levels by setting the screen intensity to ∼10^5 photons μm^{-2} s^{-1} throughout the experiment. In some experiments receptive fields were mapped using the 'filtered back projection' technique described previously (Johnston *et al.* 2014). We implemented this approach using stimulus bars 50 μm wide by 1200 μm long. The bars were flashed at 15 locations, separated by 50 μm, along a line through the centre of the receptive field traversing 700 μm. Ninety stimuli were presented to cover six presentation angles separated by 30 deg. The order of presentation was randomized to obviate adaptation effects.

Imaging and reconstruction

SBACs were dye-filled by including 0.4 % Alexa Fluor-488/594 hydrazide in the recording pipette. Retinas were fixed in 4 % paraformaldehyde for 30 min, followed by two 5 min washes in 0.1 M phosphate-buffered saline, pH 7.4. Confocal micrographs were obtained on an Olympus FV1000 confocal microscope with a ×40 or ×60 oil-immersion objective. Pairwise stitching was performed on image stacks where individual SBACs could not be contained in a single frame (Preibisch *et al.* 2009). Neuromantic 1.7.5 was used for manual 3D reconstruction of SBACs and their dendritic arbours (Myatt *et al.* 2012). The SWC output file was then imported into a morphology file for the Neuron-C simulator (Smith, 1992). Images displaying cellular morphology are maximum intensity Z-projections of an image stack.

Data analysis and statistics

Data analysis and figure preparation were performed with custom procedures in Igor Pro (Wavemetrics, Tigard, OR, USA). Code for using filtered back projection to map receptive fields was downloaded from the Igor Exchange website (Johnston *et al.* 2014).

Modelling

Passive charging curves were measured in response to ±5 mV voltage steps from a holding potential of –70 mV. At least 200 pulses in each cell were averaged to reduce synaptic noise. Summation of the average positive and negative current responses produced a flat line, indicating that voltage steps were small enough to avoid non-linearities that could be produced by activation of voltage-gated channels. The Neuron-C simulator generated a compartmental model of the cell using the morphology reconstructed from a confocal stack (Smith, 1992). The electrotonic length of the compartments was set to a short increment (<0.02λ) to preserve accuracy. Diameters of the proximal, intermediate and distal dendrites were multiplied by a normalization factor in order to match the dendritic diameters of SBACs measured from electron micrograph (EM) data at similar distances from the soma (K. Briggman, personal communication). The normalization factor was ∼0.6, implying that the dendritic diameters estimated from the confocal stacks were ∼40% thicker than those measured from EM. Soma diameter was measured as ∼11 μm.

SBACs receive tonic excitatory input under steady background illumination (Taylor & Wassle, 1995) that produces an inward current of 20–40 pA at –70 mV. We modelled the excitatory input as an array of bipolar cells (n = 140–170; density 7500 mm^{-2}; semi-random regularity mean/SD = 8). Each bipolar cell was simulated as a single compartment, and made a synapse onto the closest dendrite of the SBAC if it was within a criterion distance (typically ∼15 μm). Each bipolar cell synapse was activated by a V_{rest} slightly above the threshold for synaptic release (–45 mV) to provide a tonic excitatory current to the SBAC that totalled 20–40 pA.

In order to model the experimental responses, an 'electrode' comprising a series resistor and a capacitor was connected to the soma of the model. A fourth order Bessel filter was simulated to reproduce the low-pass filter in the recording system. The first step was to obtain estimates of the surface membrane resistivity (R_m), the cytoplasmic resistivity (R_i), the specific membrane capacitance (C_m), the electrode series resistance (R_s) and the electrode capacitance (C_e). These parameters were iteratively adjusted using a Levenberg–Marquardt (LM) least-squares procedure until the 5 mV steps applied to the compartmental model most accurately reproduced the capacitive charging curves measured in the real cell. Typically, the LM procedure required 50–300 model runs to converge upon the best fit. We ran additional simulations and found that slightly better fits were obtained with the diameter factor for proximal dendrites smaller (thinner by a factor of 0.7–0.9) than for the intermediate and peripheral dendritic regions. Therefore, we included this proximal diameter factor as

a fixed parameter in the fits. The ranges for the best fit parameter values for three cells were R_i = 17–38 Ω cm, R_m = 11,000–55,000 Ω cm^2, C_m = 0.9–1.0 μF cm^{-2} and R_s = 15–32 MΩ.

To check on the influence of the individual pattern of dendritic branching, we also fitted the model of each cell to the electrophysiology data for the other cells, and achieved relatively good fits that were close but slightly worse than for the matching electrophysiology data.

After the best-fit parameters had been determined, we performed further simulations on the models to predict the effects of dendritic filtering on the amplitude and time course of EPSCs incident upon proximal and distal dendrites. Synapses were modelled as an exponential release function (3 mV/e-fold change) driving a readily releasable pool of vesicles. Glutamate released from each vesicle activated postsynaptic cation channels defined by a ligand-activated Markov sequential-state machine (Smith, 1992; Schachter *et al.* 2010). The effect of the readily releasable pool was to create a transient input that decayed over the duration of the stimulus. The synaptic release function included a first-order low-pass filter (2 ms). The postsynaptic conductance was nominally set at 220 pS. Light stimuli were implemented by voltage-clamping the bipolar cells according to the temporal pattern of the luminance change at that point in the bipolar cell array.

Models were run on an array of 3.2 GHz AMD Opteron CPUs interconnected by Gigabit Ethernet, with a total of 200 CPU cores. Simulations of the SBAC model took 10–60 min, depending on the model complexity and duration of simulated time. The simulations were run on the Mosix parallel distributed task system under the Linux operating system. For this project, a total of ∼30,000 simulations were performed.

Results

The goal of this work was to test a model proposed for the genesis of directional signals in starburst amacrine cell dendrites, in which the kinetics of light-evoked EPSCs in SBACs vary systematically between the proximal and distal dendrites (Fig. 1). ON-type SBACs were efficiently targeted as having relatively small somas, and lacking spike responses during extracellular recordings. The identity of the cells was confirmed by filling many recorded cells with Alexa-488/594 during the recordings to visualize the dendritic morphology (Fig. 2*A*). Initially we measured currents evoked by a centred spot (200 μm diameter) at a range of holding potentials (Fig. 2*B*), in order to estimate the magnitude of the excitatory and inhibitory conductances (Fig. 2*E* and *F*). The current–voltage (*I–V*) relation of the light-evoked postsynaptic currents was essentially linear, and was generated by both excitatory and inhibitory synaptic inputs. For a light step that covered the dendritic field, the time to peak for excitation was about 110 ms (10–90% rise-time 70 ms), while inhibition reached a peak within 40 ms (10–90 % rise-time 30 ms). The excitation turned off rapidly, within about 90 ms after a light flash and undershot the baseline, while inhibition turned off more slowly, taking about 400 ms to reach the baseline. The time course of the light-evoked EPSCs shown in subsequent figures, which were recorded at the calculated chloride reversal potential (E_{Cl}), closely matches the excitatory conductance obtained from responses over a broader range of potentials, indicating that there was little contamination of the EPSCs by the concomitantly activated IPSCs.

We used measurements of EPSCs recorded at E_{Cl} to test for the predicted differences in the time course of the bipolar cell inputs as a function of dendritic location. Two methods were used to probe excitation across SBAC dendritic arbours. First we employed a newly developed technique called filtered back projection (FBP; Johnston *et al.* 2014) to measure the spatial extent of the receptive field. The light stimulus comprised light bars 50 μm × 1 mm flashed at 50 μm intervals along lines that passed through the centre of the receptive field (RF). The stimulus was repeated at six different angles separated by 30 deg. The whole stimulus set included 90 stimuli covering a roughly circular region 700 μm in diameter. The extent of the stimuli along each angle was sufficient to include the centre and part of the surround of the SBAC. The calculations provided an estimate of the strength of the synaptic inputs to the cell at a resolution of about 50 μm. Average responses from 10 cells are shown in Fig. 3. As expected the light bar stimulus produced inward current near the receptive field centre. As expected from previous work (Lee & Zhou, 2006), a significant surround response was activated outside the dendritic field. It was well-resolved in this average data, but was more difficult to see in individual responses. The antagonistic surround is evident as an inversion of the response polarity in the surround relative to the centre (inset Fig. 3*A* and *B*). The amplitude of the average responses measured at two time points as a function of stimulus location indicates that the antagonistic surround is active for both positive and negative contrast transitions (Fig. 3*B*). The calculated receptive fields for the SBACs are shown at the two time points in Fig. 3*C*. The mean diameter of the receptive field, estimated by fitting a two-dimensional Gaussian profile to the individual receptive field maps at t = 80 ms, was 166 ± 3 μm (n = 10).

In order to determine whether EPSCs were more transient at peripheral locations relative to the centre, we calculated receptive field maps at 10 ms intervals, and measured the amplitude of the responses for three regions-of-interest (ROIs). The inner ROI comprised the central four 50 × 50 μm pixels. The second and third ROIs comprised the 12 pixels surrounding the centre ROI, and the next set of pixels out (Fig. 3*D*). Moving out

from the centre, the mean amplitude calculated for the EPSCs within the ROIs declined, but after normalizing the amplitudes the time course was unchanged (Fig. 3*E*), suggesting that the bipolar cells providing proximal and distal inputs are very similar.

To corroborate this finding we used a second more direct approach to compare the time course of EPSCs at proximal and distal locations. EPSCs in the SBACs were recorded in response to annuli of increasing size (Fig. 4). The width of the annulus was held fixed at 50 μm, while the mean diameter was increased in 50 μm increments. Annuli within the RF centre produced large inward currents, which became progressively smaller as more distal inputs were activated (Fig. 4*C*, open circles). Consistent with the presence of the antagonistic surround revealed by the bar stimuli (Fig. 3), responses were inverted in the surround (Fig. 4*A*). The higher signal-to-noise of these recordings allowed for better resolution of EPSCs out to annulus diameters of 250 μm, and provided a further test of the hypothesis that bipolar cell inputs become more transient at distal input locations. However, in agreement with the data from flashed bars, the time course of the EPSCs was essentially identical regardless of distance from the soma (Fig. 4*B*), a finding that suggests that dendritic filtering has little effect on the time course of excitation in SBACs.

The magnitude of the EPSCs reflects both the density and the efficacy of the inputs across the dendritic arbour and attenuation due to incomplete space-clamp of distal inputs resulting from dendritic filtering. If dendritic filtering attenuates the amplitude of the EPSCs, then it should also slow the time course. Application of patch-electrodes to the dendrites to directly measure distal EPSCs in SBACs is not possible due to the small diameters of the processes. Therefore, we constructed computer models of SBACs and simulated EPSCs at

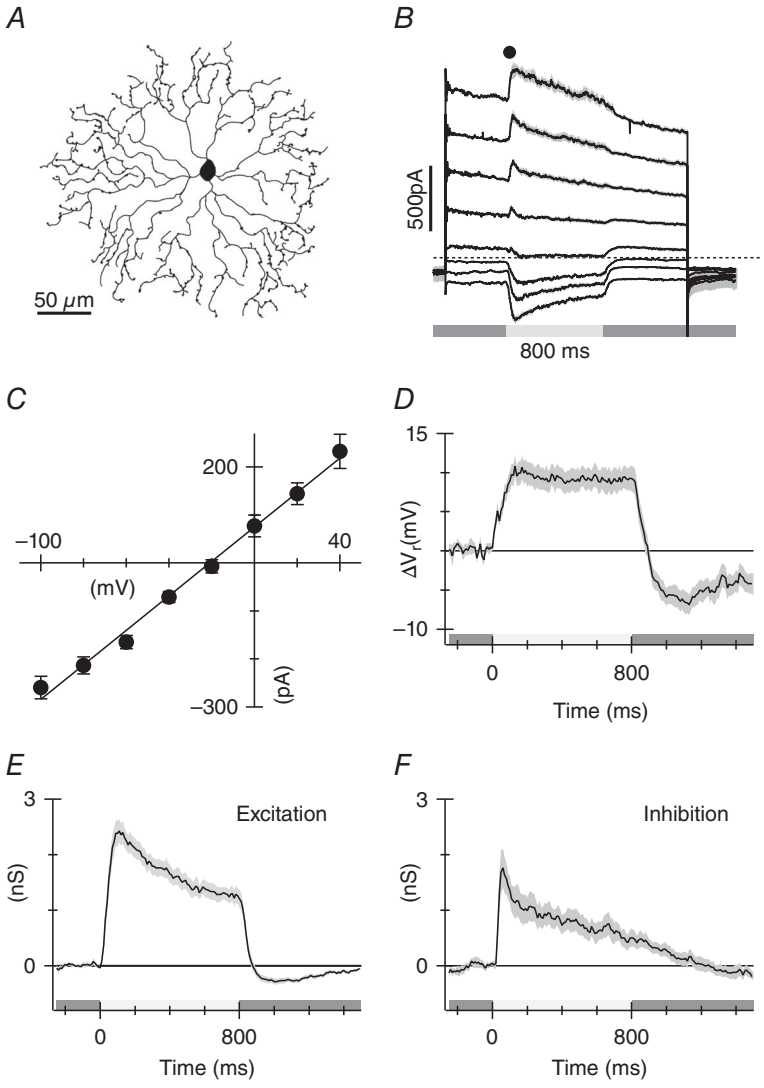

Figure 2. Light-evoked synaptic inputs to SBACs
A, line drawing from a confocal micrograph showing representative morphology of an ON-type starburst amacrine cell in the mouse. *B*, average currents recorded from 10 cells at a range of holding potentials. Stimulus was a 200 μm diameter light spot centred on the receptive field. Stimulus timing is shown beneath the traces. *C*, average amplitude (±SEM) of the light-evoked current measured at the time point shown in *B*. *D*, change in the whole-cell zero current potential produced by the light flashes. *E* and *F*, excitatory and inhibitory conductances calculated from the *I–V* relations. The grey shading shows the standard error of the mean for the measurements from the 10 cells.

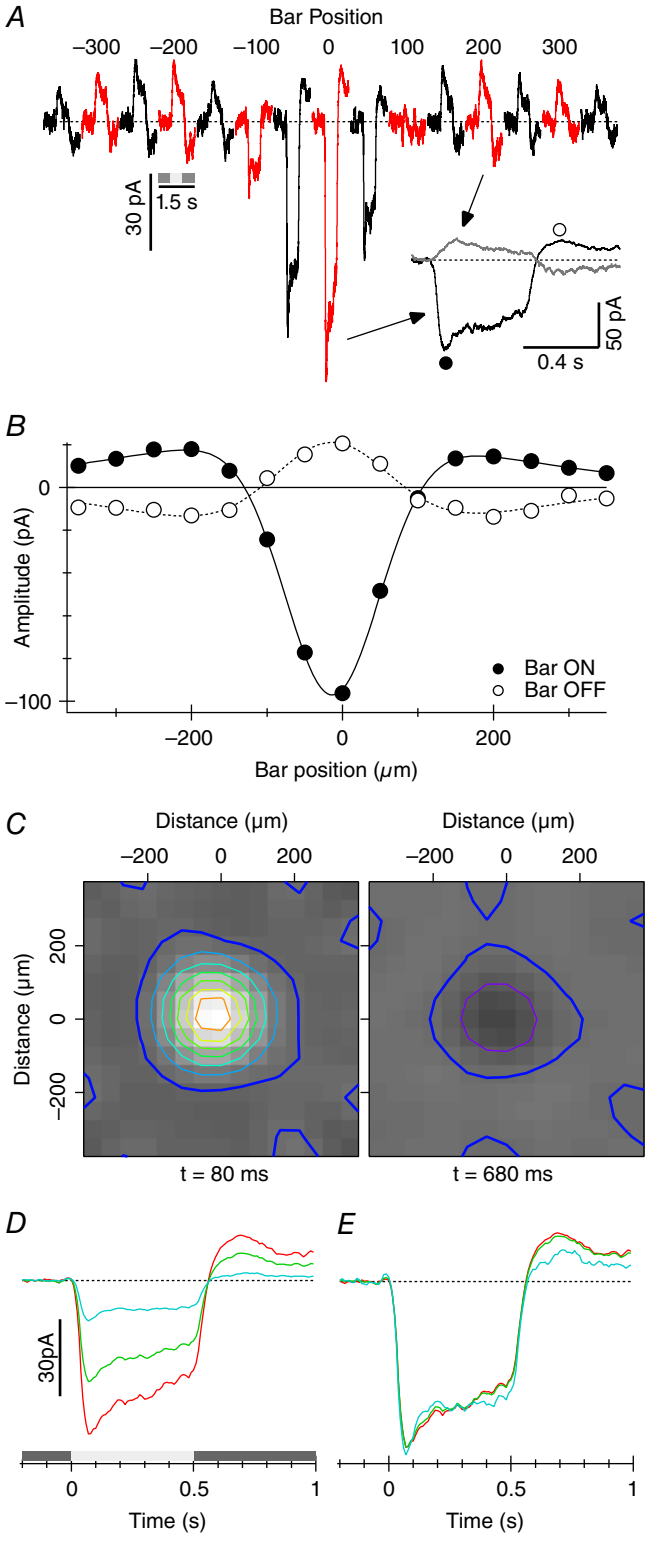

Figure 3. Receptive field of SBAC calculated by filtered back projection as described in Methods
Data represents the average from 10 cells. *A*, average responses produced by the 50 μm × 1 mm light bar at each location traversing the centre of the receptive field. Traces are averages for all six angles in the 10 cells. *B*, amplitude of the responses as a function of position measured at the two time points shown in *A*. Error bars are obscured by the symbols. The continuous line shown the best fitting difference-of-Gaussians function. The width (2σ) of the centre and surround Gaussians were 178 and 715 μm, respectively. *C*, receptive fields calculated by FBP at two time points, near the peak of the response at stimulus onset (filled circle in inset in *A*), and near the maximum for the outward current after the termination of the flash (open circle in inset in *A*). The overlaid contour lines are drawn at 10 pA intervals – the thick blue lines show the 0 pA level. Timing beneath is relative to start of the stimulus. *D*, spatial dependence of response time course calculated from the FBP data. Receptive fields were calculated at 10 ms intervals. Three regions of interest were assigned to measure the time course of the response; the central four pixels covered by the red contour line in *C*, the 12 pixels surrounding the centre (green), and the next row of pixels out (cyan). *E*, responses from *D* normalized to equate the peak amplitude.

proximal and distal locations to determine the effects of dendritic filtering on the EPSCs measured at the soma. The computer models were calibrated by pairing electrical responses with the matching dendritic morphology. Currents in response to 5 mV voltage steps were obtained from SBACs while filling the cells with Alexa dye. Morphology was digitized from confocal micrograph stacks (Fig. 4*A*). Compartmental models were constructed, including a patch-clamp electrode applied to the soma, and the 5 mV voltage steps were simulated. The simulated current transients were fitted to the measured transients by adjusting the model parameters using a least-squares algorithm. The models produced excellent predictions of the measured current transients (Fig. 5*B*; see Methods for details). The next step was to use these calibrated models to predict the effects of dendritic filtering by simulating bipolar cell synaptic input at different locations in the dendrites.

Electron microscopic studies have indicated that bipolar cell inputs are constrained to the proximal and intermediate dendrites with only sparse input on distal processes, particularly for ON SBACs (Kim *et al.* 2014; Greene *et al.* 2016). Therefore, inputs were placed within 90 μm from the soma. Figure 5*C* illustrates the rising phase of EPSCs recorded by the electrode at the soma and produced by excitatory synapses onto either proximal or distal dendrites. The amplitude of the distal EPSC was attenuated about 3-fold relative to the proximal input (compare vertical calibrations Fig. 5*C*); however, the time course of the EPSCs was slowed by ∼1 ms. Note that real EPSCs recorded at the soma have rise-times on the order of tens of milliseconds (Figs 1–3), and therefore the modelling is consistent with the data in showing that dendritic filtering will have little discernible effect on the EPSC time course. On the other hand, the model correctly predicts the attenuation of EPSC amplitude as a function of distance from the soma (Fig. 5*D*). To make this comparison we converted the EPSC amplitude from Fig. 4*C* into current per unit stimulus area. The model was constructed to have an approximately uniform density

of bipolar cells per unit stimulus area. The attenuation in EPSC amplitude predicted by the three SBAC models closely matched the real data (Fig. 4*D*).

Discussion

Our aim was to determine whether a model based on ordered inputs with characteristic kinetics could explain directional GABA release from SBACs. The model requires that EPSCs from bipolar cells impinging on peripheral dendrites should be more transient than EPSCs at locations proximal to the soma. The data demonstrate that EPSC time course is independent of dendritic location, which is consistent with recent findings (Vlasits *et al.* 2016). Overall the results indicate that the 'ordered input' model cannot explain direction-selective GABA release from ON-SBACs. A potential caveat to this conclusion is that recordings from an electrode at the soma might not accurately represent the EPSC time course at peripheral locations due to dendritic filtering. Dendritic filtering, produced by current flow through the axial resistance and the surface membrane capacitance of the dendrites, slows and attenuates EPSCs at distal locations (Rall, 1967). Thus, one possibility is that the more transient EPSCs expected at the distal locations have been slowed sufficiently by dendritic filtering so that they appear identical to EPSCs activated at proximal locations. Although such a coincidence seems unlikely, we addressed this possibility by using calibrated compartmental models of SBACs to estimate the effects of dendritic filtering. The model successfully predicted both the attenuation of the amplitude of the recorded EPSCs, and the lack of any marked effect on the time course. The modelling predicts that dendritic filtering should affect signals with rise-times in the millisecond range, which is an order of magnitude faster than the light-evoked EPSCs.

If the proposed ordered-input model for directional responses does not apply to ON-SBACs does this imply that the ON and OFF pathways use different circuit mechanisms or is it possible that the model does not

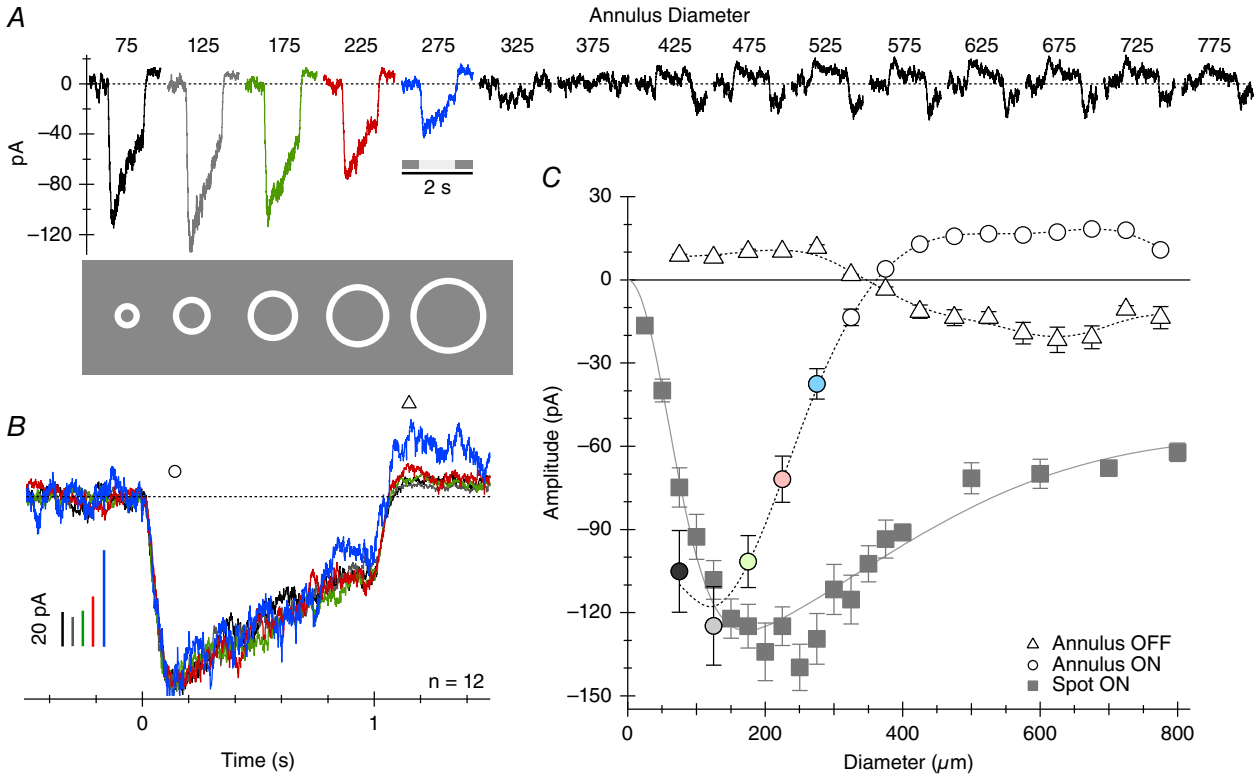

Figure 4. EPSCs recorded at the chloride reversal potential in response to annuli of increasing size
A, average responses from 12 cells. The relative sizes of the first five stimuli are illustrated below the traces. The width of the annuli were fixed at 50 μm, and the mean diameter was increased in 50 μm increments from 75 μm (ID = 50 μm, OD = 100 μm) up to 325 μm. Contrast was held constant at 80%. *B*, the first five responses from *A* are superimposed and amplitudes normalized to compare the time course of the EPSCs. *C*, EPSC amplitude as a function of annulus diameter. Open circles and triangles were measured at the time points indicated by the corresponding symbols in *B*. The symbol colours correspond to the traces in *A*. The grey squares show the average peak responses for a series of spots of increasing diameter in the same 12 cells. The continuous line shows the best fitting difference-of-Gaussians function. The width (2σ) of the centre and surround Gaussians were 172 ± 23 and 930 ± 215 μm, respectively.

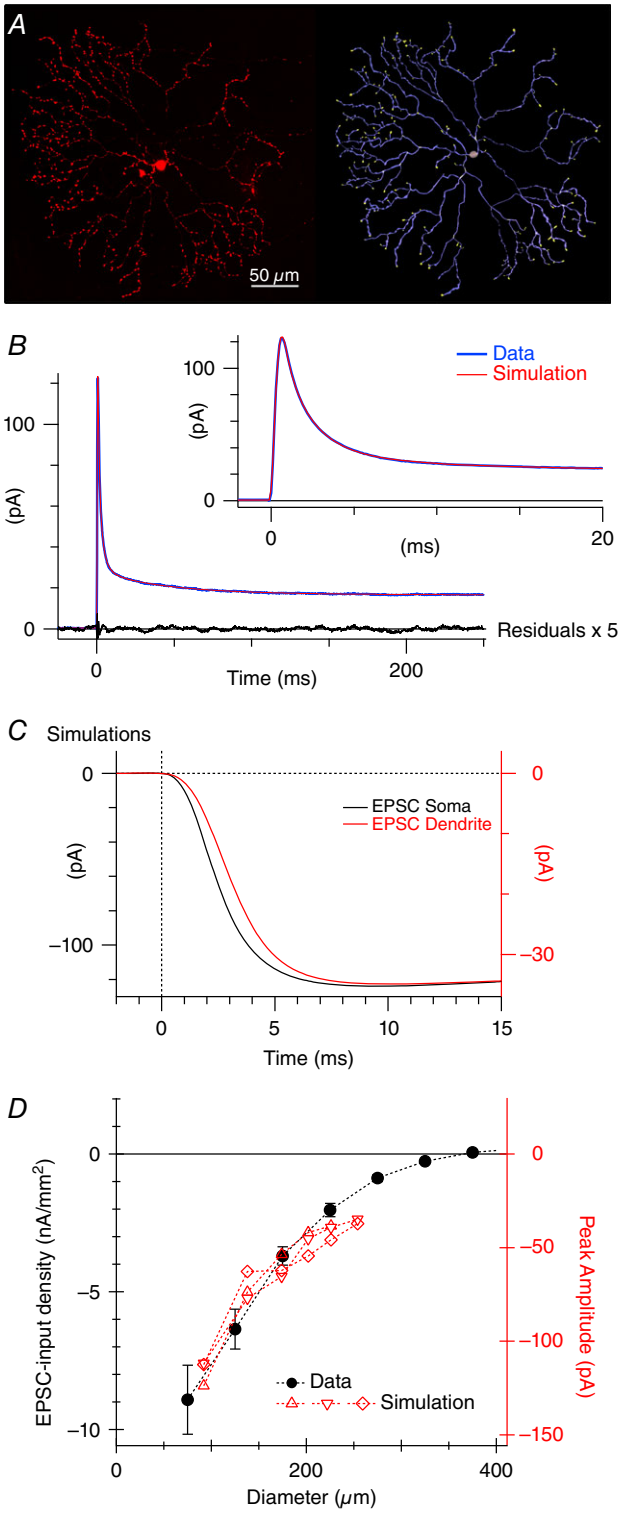

Figure 5. Simulations demonstrating that the EPSC time course is not limited by dendritic filtering
A, a confocal micrograph of an SBAC fluorescently labelled with Alexa dye (left) and the corresponding digitized morphology used for simulations (right). *B*, current responses to a 5 mV voltage step. Two hundred positive and inverted negative responses were averaged (blue). The biophysical parameters in the compartmental model were adjusted to obtain the best fit (red overlay, see Methods). The black line shows the residuals after subtracting the fit from the data. The residuals are shown at a 5-fold higher gain and indicate that there was no systematic deviation between the model prediction and the data. *C*, current traces produced by excitatory conductance applied to the soma (black) or the peripheral dendrites (red). Note the 3-fold difference in the vertical scaling required to normalize the amplitudes. The current recorded at the soma was attenuated due to electrotonic decay in the dendrites, but the time course was only slightly delayed and slowed. Similar results were obtained in two other cells. *D*, filled symbols show the peak amplitude of the EPSCs (open circles in Fig. 4*C*) normalized for stimulus area. The red symbols show the amplitude of simulated EPSCs in the three reconstructed cells produced by conductances applied at various distances from the soma (black). There is good agreement with the real data (red).

apply to either pathway? Two factors should be considered. First, for the EM study supporting the model, the tissue was treated to remove intracellular structures in order to facilitate tracing of plasma membrane profiles in the micrographs (Briggman *et al.* 2011; Kim *et al.* 2014; Greene *et al.* 2016). A disadvantage of this approach was the inability to recognize synaptic connections based on intracellular ultrastructure, instead relying on contact area as an estimate of connectivity. However, effort was made to validate this approach by comparing the contact analyses of SBAC to DSGC connections to a similar analysis in conventionally fixed sample. A second point to consider is that the kinetic characterizations of cone bipolar cell types differ in imaging versus electrophysiological studies. The ordered-input model for ON-SBACs, requires that the BC-7 bipolar cells that make proximal inputs are more sustained than the BC-5 bipolar cells at distal locations. These kinetic categorizations were based on calcium imaging of BC terminals, which assumes that the bulk Ca^{2+} concentration is an accurate proxy for transmitter release (Baden *et al.* 2012). More direct measurements of transmitter release were made using the genetically encoded glutamate sensor, iGluSnFr (Borghuis *et al.* 2013). These imaging studies support the view that transient cells tend to ramify in the mid-IPL with more sustained cells restricted to the outer region (Awatramani & Slaughter, 2000; Ichinose *et al.* 2005; Euler *et al.* 2014), but do not unambiguously resolve the glutamate release properties of specific bipolar cell types. Current clamp recordings from ON BCs identified BC7 as one of the most transient subtypes (Ichinose *et al.* 2014). Similarly, analysis of light-evoked EPSPs in mouse OFF cone bipolar cells classified both BC2 and BC3a as transiently responding (Ichinose & Hellmer, 2015). If the glutamate release time course from these various bipolar cells reflects the voltage responses, then the proposed ordered-input model may not be tenable. Taken together, these previous results and the data presented here, suggest that the ordered-input model may not be applicable to either the OFF or ON SBACs.

Ultrastructural analysis shows that bipolar cell inputs onto ON SBACs extend out to about 90 μm from the soma and are sparse on distal processes (Kim *et al.* 2014; Greene *et al.* 2016), a finding that has been functionally confirmed using high spatial resolution mapping of glutamate receptors on these cells (Vlasits *et al.* 2016). Our receptive field maps revealed responses out to ∼125 μm from the soma (Fig. 4*A*), slightly beyond the anatomical extent of bipolar cell inputs to SBACs. Such an apparent discrepancy might result if the soma, which is centred on the stimulus, was not perfectly concentric within the dendritic arbour. In addition, the width of the bipolar cell receptive fields could expand the extent of light-evoked inputs (Berntson & Taylor, 2000; Kuo *et al.* 2016).

The findings do not rule out a weaker version of the ordered-input model, which entails progressive or ordered activation of identical EPSCs within the dendrites of SBACs that can produce a directional bias in the SBAC dendritic tips (Tukker *et al.* 2004; Vlasits *et al.* 2016). Tukker *et al.* (2004) proposed that the directional signal is produced by interaction between a 'global' signal, produced across the dendritic arbour, and the local signal generated in the dendritic tips. The model does not rely on the temporal properties of the bipolar cell inputs, but rather shows that given appropriate electrotonic attenuation along the dendrites, a larger voltage response is produced in the distal dendrites when the stimulus moves from the soma towards the tip than when the stimulus moves from the tip towards the soma. Such directional signals might be amplified by several mechanisms, including reciprocal inhibition between oppositely directed SBAC dendrites (Lee & Zhou, 2006; Lipin *et al.* 2015; Pei *et al.* 2015; Vlasits *et al.* 2016), and possibly also regenerative amplification due to activation of sodium or calcium channels in the distal dendrites (Cohen, 2001; Euler *et al.* 2002; Oesch & Taylor, 2010).

References

Awatramani GB & Slaughter MM (2000). Origin of transient and sustained responses in ganglion cells of the retina. *J Neurosci* **20**, 7087–7095.

Baden T, Berens P, Bethge M & Euler T (2012). Spikes in mammalian bipolar cells support temporal layering of the inner retina. *Curr Biol* **23**, 1–5.

Barlow HB & Hill RM (1963). Selective sensitivity to direction of movement in ganglion cells of the rabbit retina. *Science* **139**, 412–414.

Barlow HB, Hill RM & Levick WR (1964). Rabbit retinal ganglion cells responding selectively to direction and speed of image motion in the rabbit. *J Physiol* **173**, 377–407.

Berntson A & Taylor WR (2000). Response characteristics and receptive field widths of on-bipolar cells in the mouse retina. *J Physiol* **524**, 879–889.

Borghuis BG, Marvin JS, Looger LL & Demb JB (2013). Two-photon imaging of nonlinear glutamate release dynamics at bipolar cell synapses in the mouse retina. *J Neurosci* **33**, 10972–10985.

Briggman KL, Helmstaedter M & Denk W (2011). Wiring specificity in the direction-selectivity circuit of the retina. *Nature* **471**, 183–188.

Caldwell JH, Daw NW & Wyatt HJ (1978). Effects of picrotoxin and strychnine on rabbit retinal ganglion cells: lateral interactions for cells with more complex receptive fields. *J Physiol* **276**, 277–298.

Cohen ED (2001). Voltage-gated calcium and sodium currents of starburst amacrine cells in the rabbit retina. *Vis Neurosci* **18**, 799–809.

Enciso GA, Rempe M, Dmitriev AV, Gavrikov KE, Terman D & Mangel SC (2010). A model of direction selectivity in the starburst amacrine cell network. *J Comput Neurosci* **28**, 567–578.

Euler T, Detwiler PB & Denk W (2002). Directionally selective calcium signals in dendrites of starburst amacrine cells. *Nature* **418**, 845–852.

Euler T, Haverkamp S, Schubert T & Baden T (2014). Retinal bipolar cells: elementary building blocks of vision. *Nat Rev Neurosci* **15**, 507–519.

Fried SI, Munch TA & Werblin FS (2002). Mechanisms and circuitry underlying directional selectivity in the retina. *Nature* **420**, 411–414.

Greene MJ, Kim JS & Seung HS (2016). Analogous convergence of sustained and transient inputs in parallel on and off pathways for retinal motion computation. *Cell Rep* **14**, 1892–1900.

Hausselt SE, Euler T, Detwiler PB & Denk W (2007). A dendrite-autonomous mechanism for direction selectivity in retinal starburst amacrine cells. *PLoS Biol* **5**, e185.

Ichinose T, Fyk-Kolodziej B & Cohn J (2014). Roles of on cone bipolar cell subtypes in temporal coding in the mouse retina. *J Neurosci* **34**, 8761–8771.

Ichinose T & Hellmer CB (2015). Differential signalling and glutamate receptor compositions in the OFF bipolar cell types in the mouse retina. *J Physiol* **594**, 883–894.

Ichinose T, Shields CR & Lukasiewicz PD (2005). Sodium channels in transient retinal bipolar cells enhance visual responses in ganglion cells. *J Neurosci* **25**, 1856–1865.

Johnston J, Ding H, Seibel SH, Esposti F & Lagnado L (2014). Rapid mapping of visual receptive fields by filtered back projection: application to multi-neuronal electrophysiology and imaging. *J Physiol* **592**, 4839–4854.

Kim JS, Greene MJ, Zlateski A, Lee K, Richardson M, Turaga SC, Purcaro M, Balkam M, Robinson A, Behabadi BF, Campos M, Denk W & Seung HS (2014). Space–time wiring specificity supports direction selectivity in the retina. *Nature* **509**, 331–336.

Kittila CA & Massey SC (1997). Pharmacology of directionally selective ganglion cells in the rabbit retina. *J Neurophysiol* **77**, 675–689.

Kuo SP, Schwartz GW & Rieke F (2016). Nonlinear spatiotemporal integration by electrical and chemical synapses in the retina. *Neuron* **90**, 1–13.

Lee S, Kim K & Zhou ZJ (2010). Role of ACh-GABA cotransmission in detecting image motion and motion direction. *Neuron* **68**, 1159–1172.

Lee S & Zhou ZJ (2006). The synaptic mechanism of direction selectivity in distal processes of starburst amacrine cells. *Neuron* **51**, 787–799.

Lipin MY, Taylor WR & Smith RG (2015). Inhibitory input to the direction-selective ganglion cell is saturated at low contrast. *J Neurophysiol* **114**, 927–941.

Myatt DR, Hadlington T, Ascoli GA & Nasuto SJ (2012). Neuromantic – from semi-manual to semi-automatic reconstruction of neuron morphology. *Front Neuroinform* **6**, 4.

Oesch NW & Taylor WR (2010). Tetrodotoxin-resistant sodium channels contribute to directional responses in starburst amacrine cells. *PLoS One* **5**, e12447.

Ozaita A, Petit-Jacques J, Volgyi B, Ho CS, Joho RH, Bloomfield SA & Rudy B (2004). A unique role for Kv3 voltage-gated potassium channels in starburst amacrine cell signaling in mouse retina. *J Neurosci* **24**,7335–7343.

Pei Z, Chen Q, Koren D, Giammarinaro B, Acaron Ledesma H & Wei W (2015). Conditional knock-out of vesicular GABA transporter gene from starburst amacrine cells reveals the contributions of multiple synaptic mechanisms underlying direction selectivity in the retina. *J Neurosci* **35**, 13219–13232.

Preibisch S, Saalfeld S & Tomancak P (2009). Globally optimal stitching of tiled 3D microscopic image acquisitions. *Bioinformatics* **25**, 1463–1465.

Rall W (1967). Distinguishing theoretical synaptic potentials computed for different soma-dendritic distributions of synaptic input. *J Neurophysiol* **30**, 1138–1168.

Schachter MJ, Oesch N, Smith RG & Taylor WR (2010). Dendritic spikes amplify the synaptic signal to enhance detection of motion in a simulation of the direction-selective ganglion cell. *PLoS Comput Biol* **6**, e1000899.

Smith RG (1992). NeuronC: a computational language for investigating functional architecture of neural circuits. *J Neurosci Methods* **43**, 83–108.

Taylor WR & Wassle H (1995). Receptive field properties of starburst cholinergic amacrine cells in the rabbit retina. *Eur J Neurosci* **7**, 2308–2321.

Tukker JJ, Taylor WR & Smith RG (2004). Direction selectivity in a model of the starburst amacrine cell. *Vis Neurosci* **21**, 611–625.

Vlasits AL, Morrie RD, Tran-Van-Minh A, Bleckert A, Gainer CF, DiGregorio DA & Feller MB (2016). A role for synaptic input distribution in a dendritic computation of motion direction in the retina. *Neuron* **89**, 1317–1330.

Wyatt HJ & Daw NW (1976). Specific effects of neurotransmitter antagonists on ganglion cells in rabbit retina. *Science* **191**, 204–205.

Yoshida K, Watanabe D, Ishikane H, Tachibana M, Pastan I & Nakanishi S (2001). A key role of starburst amacrine cells in originating retinal directional selectivity and optokinetic eye movement. *Neuron* **30**, 771–780.

Additional information

Competing interests

The authors declare no competing financial interests.

Author contributions

T.S., R.G.S. and W.R.T. designed the research, analysed the data, and wrote the paper. T.S. performed the physiological experiments and the anatomical reconstructions, and W.R.T. and R.G.S. performed the computer modelling. All authors have approved the final version of the manuscript and agree to be accountable for all aspects of the work. All persons designated as authors qualify for authorship, and all those who qualify for authorship are listed.

Funding

This research was supported by NIH grants R01 EY022070, P30 EY010572 and P30 NS061800; and by unrestricted funding to Casey Eye Institute from Research to Prevent Blindness (New York, NY).

Acknowledgements

We thank Dr Lisa Coussens for generously supplying mice used in this experiment and Dr Teresa Puthussery for helpful discussions and critical reading of the manuscript.